Progress In Electromagnetics Research Letters, Vol. 92, 39–45, 2020

The Deployment of Stub Structures for Mutual Coupling Reduction in MIMO Antenna Applications

Chuanhui Hao[1], Hongmei Zheng[2], Jingjing Zhang[1], and Xubao Sun[1, *]

Abstract—This paper presents a practical scheme for threefold stubs etched on the ground plane (GP) to reduce mutual coupling between adjacent patching elements. The multiple input multiple output (MIMO) antenna array consists of two concentric polyhedron annulus patches, a conventional dielectric substrate, threefold fork-shaped stubs (TFSS), and a microstrip line feeder. The results of previous case studies indicate that the mutual coupling about 5 dB to 47 dB was reduced from 8 GHz to 9.3 GHz ($S_{11} < -10$ dB) for antenna arrays. The capabilities of the antenna (in envelope correlation coefficient = 0.018, voltage standing wave ratio = 1.2892, and diversity gain = 20 dB) have been confirmed at center frequency of 8.97 GHz. An examination of TFSS antennas shows that the side lobes in both the E-plane and H-plane descends alongside an increasingly broad radiation pattern. The above results demonstrate that the proposed design is highly efficient in MIMO antenna applications.

1. INTRODUCTION

With the advent of mobile internet, an upsurge in video data traffic among users of mobile devices has given rise to high demand for broad-spectrum and energy efficiency antenna technology. Multiple input multiple output (MIMO) antennas hold great potential for utilization in wireless devices, enabling the installation of multiple antennas to generate stable data streams between transmitters and receivers. With MIMO chips and Wi-Fi pattern compliance standards, MIMO antennas could facilitate communication via the chip itself or 802.11a Wi-Fi equipment, at 108 Mbps and 54 Mbps, respectively [1]. However, higher mutual coupling occurs in MIMO antenna array elements when higher message accounting transmission rates are handled. The primary cause of higher degrees of mutual coupling between the array elements is the distortion of current distribution due to the undesired generation of surface waves within the substrate. In other words, monopole interactions prevent the formation of grating lobes due to $l < \lambda_0/2$ (l represents the spatial distance between the antenna elements; λ_0 represents the free space wavelength) which, in turn, results in input impedance mismatching. Consequently, mutual coupling hinders the performance of MIMO antennas in terms of side-lobe formation, beam-scanning capability, SNR (signal to noise ratio), and ECC (envelope correlation coefficient).

In previous studies, several techniques have been employed to mitigate the hindrance mentioned above, such as EBG (electromagnetic band gap) [2, 3], metal slabs [4], DGS (defective ground structure) [5, 6], and rectangular slot(s) [7, 8]. The drawbacks of these techniques are that they engender backward signal leakage and occupy large amounts of space. In material science, magnetic metamaterial has been used in low-coupling antenna designs, including CSRR (complementary

Received 21 October 2019, Accepted 2 June 2020, Scheduled 15 June 2020

* Corresponding author: Xubao Sun (hchh518666@sina.com).

[1] College of Electrical Engineering and Automation, Shandong University of Science and Technology, Qian Wan Gang Road, No. 579, Qingdao 266590, China. [2] Hongmei Zheng was with School of Science, Yanshan University, China. She is now with the Sun City Middle School in Dezhou, Economic Development Zone, Dezhou, China.

split-ring resonator) [11], CLL (capacitive loaded loop) [13], metalization [14], and the use of π-shaped elements [15]. Although the techniques mentioned above effectively reduce the occurrence of surface waves, the array antennas still generate multiple wavelengths in horizontal and perpendicular orientations. However in [17], the high coupling about $S_{21} \approx -5\,\text{dB}$ at 7.5–9.5 GHz of FDN (frequency diplexer network) has been produced in MIMO wireless parallel data transmission.

In the model proposed in this paper, the spacing of the concentric polyhedron annulus elements is smaller, and the overall cost is lower than that of the scheme in [17] where the TFSS structure is etched onto the GP back layer. Mutual coupling reduction is achieved here by routing the surface wave current topology orientation in an overall planar configuration. The proposed GP stub structures serve to reduce side-lobe radiation generated in the E-plane without incurring cross polarisation as primitive antennas do. ANSYS High-Frequency Structure Simulator (HFSS) software is utilized to simulate, analyse, and optimize the prototype design. The simulation and measurement results are satisfactory in terms of S_{11}, S_{21}, envelope correlation coefficient (ECC), diversity gain, current distribution, voltage standing wave ratio (VSWR), radiation patterning, and peak realized gain. The antenna's complete design process and circuit analysis are explored in Section 2. The antenna's properties, along with the simulation and measurement results, are presented in Section 3. Finally, the conclusion follows in Section 4.

2. ANTENNA DESIGN AND CURRENT DISTRIBUTION

As shown the model in Fig. 1 using HFSS software, the antenna's geometry was drawn using a TFSS band-stop property etched onto the GP. The MIMO antenna substrate with $wa = 34\,\text{mm}$ and $la = 22\,\text{mm}$ consists of a low-cost conventional FR4_epoxy material with the parameters of $\varepsilon_r = 4.4$, $\tan\delta = 0.02$, and substrate thickness of $h1 = 1.5\,\text{mm}$. The patching of the two concentric polyhedron annuli with a thickness of $h2 = 0.032\,\text{mm}$ was designed using a microstrip line feeder. The rectangular and fork patches as ground plane are printed in the back layer [Fig. 1(b)], in which the dimension is shown in Table 1. As a direct conclusion of using the cyclo-patch to design antenna radiation layer,

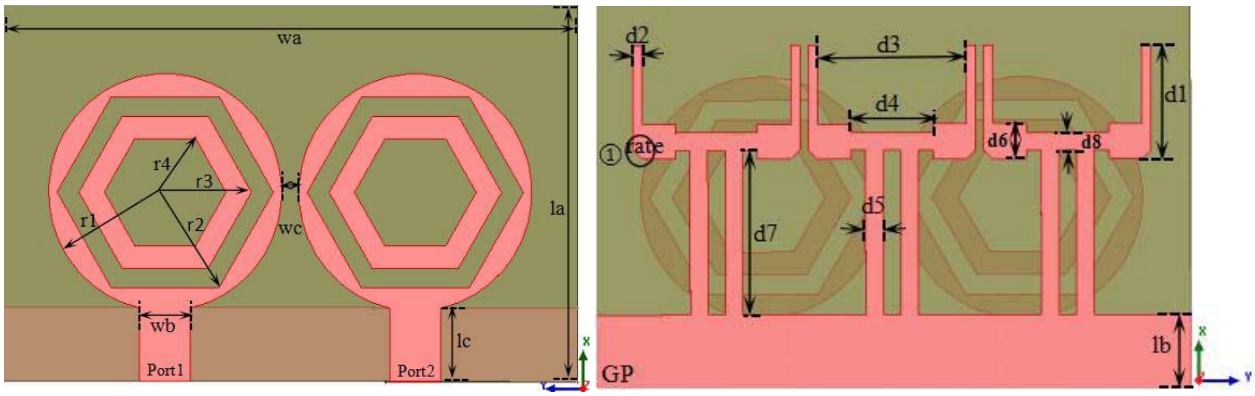

Figure 1. Proposed TFSS schematic: (a) Top layer with $wa = 34$; (b) Back layer.

Table 1. Design dimensions of antenna parameters.

Scalar	Value (mm)	Scalar	Value (mm)	Scalar	Value (mm)	Scalar	Value (mm)
wb	3.0	$r4$	3.6	$d8$	1.01	lc	4.3
wc	1.0	$d1$	6.5	$r1$	6.9	$d4$	4.7
lb	4.3	$d2$	0.5	$d5$	1.0	$d6$	2.0
$r3$	5.1	$d3$	8.5	$r2$	6.4	$d7$	9.4

one can expect that this method can increase the effective current length, and secondly, cyclo-patch antenna is easier to minimize. For cyclo-patch antenna with radius of $r1 \times r4$ [Fig. 1(a)], the electric field intensity beneath the patch varies as the two concentric polyhedron annuli [19]. To achieve a lower value of coupling in the centre frequency ($f_0 = 8.97\,\text{GHz}$), the angular rate was set during the corner cutting process. Thus, an angular rate of 0.2 for the copper material was used in Table 1 of Fig. 1(b) during the HFSS software simulation. The forked shape functions as a band-stop filter to reduce the coupling power among the different elements. The experiment shows that the number of TFSSs is $n = 3$, thereby achieving an ideal S-parameter of 8.97 GHz. The distance between the patches is $\lambda_0/33.44$ (1 mm). The design dimensions of the optimized parameters (including the top-layer patch and back-layer forked shape) are summarized in Table 1.

Through the analysis of current distribution at 8.97 GHz presented in Fig. 2, it can be inferred that the circuit shorts to the GP at Port 2 (to any I1 or I2) when V2 = 0. Namely, the left microstrip patch is excited upon consolidating voltage (V1), and an additional current is excited on the right microstrip patch.

Based on [18], it means that the effective electrical length increases in ground plane and that resonance frequency decreases, and therefore, the current on the reflector flows along TFSS path which results in surface wave reduction. In Fig. 2, since currents I1 and I2 are distributed via parallel connection, the current wave is suppressed by the equivalent band-stop filtering function of the TFSS, in which a large portion of current is trapped by TFSS. Consequently, the inserted TFSS reflects the current wave, thereby reducing the coupling impact between the antenna cells.

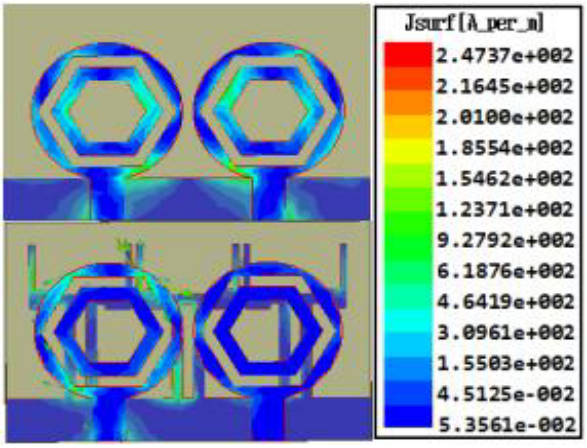

Figure 2. Current distribution.

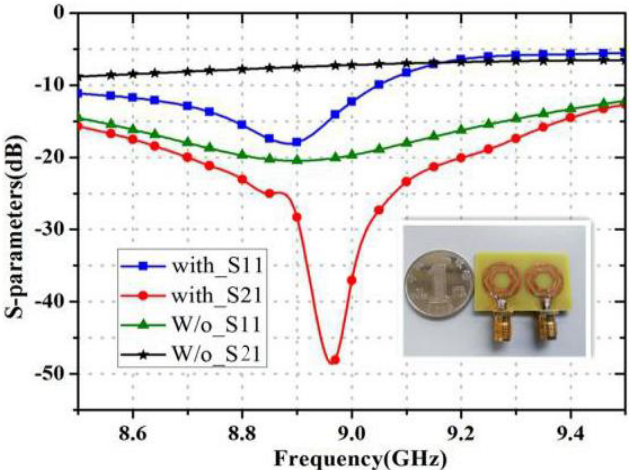

Figure 3. Simulation results comparison.

3. SIMULATION AND DISCUSSION

To evaluate the antenna's performance, its simulated results (obtained using HFSS software) with and without TFSS are depicted in Fig. 3 (where X represents the frequency, and Y represents the S-parameters). Using TFSS, the minimal coupling value is roughly $S_{21} = -55.12\,\text{dB}$ within the 8.97 GHz frequency point, thereby reducing the degree of mutual coupling to 47.8 dB (compared to $-7.26\,\text{dB}$ at 8.97 GHz without TFSS). The impedance bandwidth of the antenna is calculated at approximately 15.02% ($S_{11} < -10\,\text{dB}$) between 8.0 GHz and 9.3 GHz. Meanwhile, the ADS simulation indicates a matching load impedance of $ZL = Z0 * (-1.038 + j0.644)$ in $S_{11} = -18.29\,\text{dB}$ at 8.97 GHz. Fig. 4 shows that the number of TFSS is $n = 3$ getting ideal S-parameters at 8.97 GHz. (here, S-parameter of $n = 1$ is only the central fork; $n = 2$ is the balanced forks on both sides).

In contrasting the simulation results with and without TFSS, the main radiation patterns of co-polarization within the Phi = 0° and 90° planes are plotted in Figs. 5(a)& (b). The results indicate that the proposed antenna's radiation pattern of co-polarization is more symmetrical and round-shaped

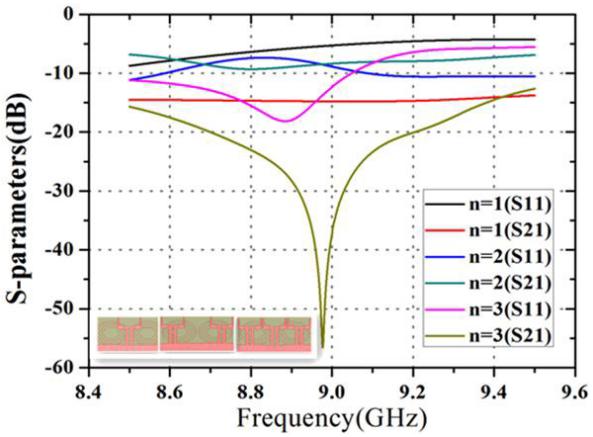

Figure 4. Number comparison of design TFSS.

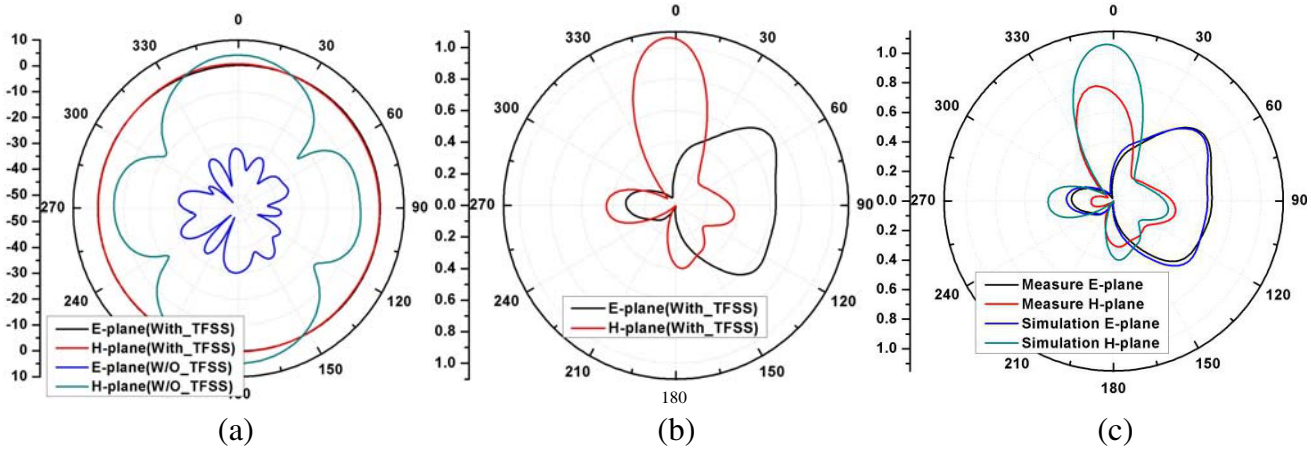

Figure 5. Main radiation pattern in E/H plane of at 8.97 GHz. (a) Simulated data comparison of antenna loaded with and W/O TFSS. (b) Simulated data with TFSS. (c) Simulated and measured data comparison.

with comprehensive radiation than that without TFSS (as shown Fig. 5(a)). The simulation results also indicate that the radiation efficiency maximal value is 86.96% with a gain of 1.05 dBi within Theta = 0° of H-plane in Fig. 5(b). Introducing additional oscillator current elements at 0° increases directivity. In Fig. 6(a), it is observed that the test coupling point shifts a little to higher than simulated result at 8.97 GHz. And the undesired radiation pattern of co-polarization is observed mainly in the H-plane in Fig. 5(c), with the simulated and measured radiation patterns at frequency points of 8.97 GHz. The errors both in fabrication and measurement can cause the slight discrepancy of simulated and measured results. A photograph of the fabricated and measured prototype is shown in Fig. 6(b).

In Table 2, the proposed design is compared to other designs from the research literature. The table indicates that the proposed design demonstrates satisfactory impedance matching performance, ultra-wideband performance, and stability gain coefficient. Therefore, the proposed MIMO antenna array design would be of benefit to the development of transmission technology.

Diversity and multiplexing characteristics constitute the major aspects of the principal functioning of both ECC and DG. As per the following equation, the proposed MIMO antenna design's ECC is below 0.5 [20], thereby substantiating its satisfactory performance:

$$\mathrm{ECC} = \frac{\left|S_{11}^{*}S_{12} + S_{21}^{*}S_{22}\right|^{2}}{\left[1 - \left(\left|S_{11}\right|^{2} + \left|S_{21}\right|^{2}\right)\right]\left[1 - \left(\left|S_{22}\right|^{2} + \left|S_{12}\right|^{2}\right)\right]}, \tag{1}$$

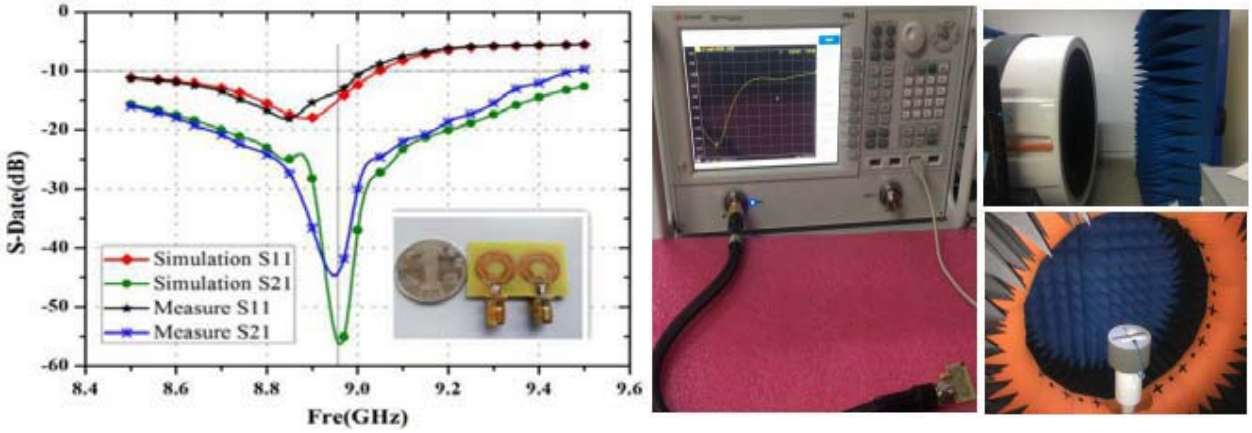

Figure 6. Simulated and measured data comparison of antenna loaded with TFSS. (a) S-parameters comparison. (b) Photograph of the measure prototype.

Table 2. Comparative results with reference to this paper.

Paper	Reduction method	Reduction [dB]	Dimension	gain [dBi]	Radiation efficiency [%]	ECC	VSWR
[2]	EBG	21.25	$1.56\lambda_0 \times 0.30\lambda_0$	9.11	91	0.015	1.55
[5]	DGS	39	$0.22\lambda_0 \times 0.31\lambda_0$	4.8	no	no	1.25
[9]	system method	16	$0.47\lambda_0 \times 0.27\lambda_0$	no	63	no	1.75
[10]	SRRS	8 to 27	$0.56\lambda_0 \times 0.38\lambda_0$	5	80	0.08	no
[13]	CLL	40	$0.51\lambda_0 \times 0.45\lambda_0$	6.2	97	0.03	1.8
[12]	Rectangular patch	25	$0.31\lambda_0 \times 0.21\lambda_0$	1.5	92	< 1	no
[16]	MSS	10 to 34	$0.44\lambda_0 \times 0.32\lambda_0$	no	no	< 0.005	no
work	TFSS	43	$0.24\lambda_0 \times 0.18\lambda_0$	4.5	86.96	0.018	1.49

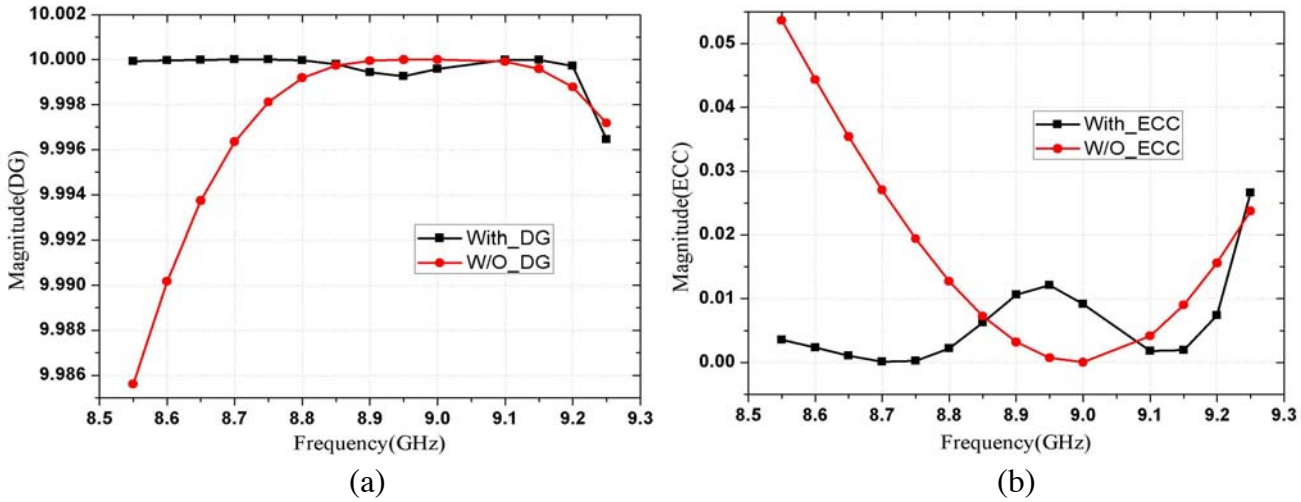

Figure 7. Compared MIMO antenna performance: (a) DG, (b) ECC.

$$\mathrm{DG} = 10\sqrt{1-(\mathrm{ECC})^2}, \tag{2}$$

Derived from the S-parameters using Eq. (1), the value of the calculated ECC is lower (near 0.03) across the -10 dB bandwidth (as shown in Fig. 7(b)) contrasting that without TFSS. Additionally, the diversity performance of DG in Eq. (2) (calculated using finite-difference time-domain software) is very high (DG $\approx$ 10 dB from 8.55 to 9.27 GHz with TFSS), as shown in Fig. 7(a). Compared to that without TFSS, both ECC and DG of the proposed structure demonstrate a stable multiplexing efficiency. To better understand the MIMO antenna's mechanism, a satisfactory input impedance matching performance (VSWR < 1.6) can be achieved across a wide frequency range of 8.7–9.0 GHz. Moreover, reflection coefficient magnitudes of about 20% and 1.7% were observed in VSWR = 1.4902 and 1.2242 with and without TFSS within the center frequency of 8.97 GHz, respectively [21].

4. CONCLUSION

To reduce mutual coupling for FDN optimization of MIMO with stable radiation patterns between 8.5 and 9.5 GHz, a threefold stub MIMO antenna design has been outlined in this paper. The design's equivalent filtering function suppresses surface current waves. The optimization results indicate that the TFSS structure effectively reduces mutual coupling without affecting other performance metrics (e.g., operating at higher frequencies, lower side-lobes, overall beam-scanning, ECC, and high-gain). Therefore, the proposed design model holds unique and practical value for the development of MIMO antennas.

ACKNOWLEDGMENT

This work was supported in Natural Science Foundation of Shandong Province ZR2013FM018.

REFERENCES

1. Morse, J., "Airgo pushing true MIMO technology," *RCR Wireless News*, Vol. 25, No. 37, 3, 2006.
2. Fritz, E. and H. J. Aguilar, "Mutual coupling reduction of two 2×1 triangular-patch antenna array using a single neutralization line for MIMO-application," *Electromagnetics*, dol: 10.13164/re, 2018.
3. Naderi, M., F. B. Zarrabi, F. S. Jafari, and S. Ebrahimi, "Fractal EBG structure for shielding and reducing the mutual coupling in microstrip patch antenna array," *AEU-International Journal of Electronics and Communications*, Vol. 93, 261–267, 2018.
4. Cole, A. J., "Mutual coupling reduction of MIMO antenna for satellite services and radio altimeter applications," *International Journal of Advanced Computer Science and Applications*, Vol. 9, No. 4, 2018.
5. Zhao, L. and K. Wang, "The MIMO antenna array with mutual coupling reduction and cross-polarization suppression by defected ground structures," *Radioengineering*, Vol. 27, No. 4, 969–975, 2018.
6. Yang, U., J. Li, S. G. Zhou, et al., "A wide-angle E-plane scanning linear array antenna with wide beam elements," *IEEE Antennas Wirel. Propag. Lett.*, 2923–2926, 2017.
7. Mojtaba, K. K. and R. H. Hamid, "Wide scan phased array patch antenna with mutual coupling reduction," *IET Microw. Antennas Propag.*, Vol. 12, 1932–1938, 2018.
8. Chi, Y. C., M. Senior, X. Fang, and D. Murch, "Mutual coupling reduction of rotationally symmetric multiport antennas," *IEEE Trans. Antennas Propag.*, Vol. 66, No. 10, 5013–5021, 2018.
9. Wang, Z. Y. and L. Y. Zhu, "A meta-surface antenna array decoupling method for mutual coupling reduction in a MIMO antenna system," *Scientific Reports*, Vol. 8, No. 1, dol: 10.1038, 2018.
10. Qamar, Z., U. Naeem, S. A. Khan, M. Chongcheawchamnan, and M. F. Shafifique, "Mutual coupling reduction for high performance densely packed patch antenna arrays on finite substrate," *IEEE Trans. Antennas Propag.*, Vol. 64, No. 5, 1653–1660, May 2016.
11. Ghosh, J., D. Mitra, and S. Das, "Mutual coupling reduction of slot antenna array by controlling surface wave propagation," *IEEE Trans. Antennas Propag.*, Vol. 67, No. 2, 1352–1357, 2019.

12. Babashah, H., H. R. Hassani, and S. Mohammad-Ali-Nezhad, "A compact UWB printed monopole MIMO antenna with mutual coupling reduction," *Progress In Electromagnetics Research C*, Vol. 91, 55–67, 2019.
13. Xu, K. D., S. Wei, and A. Li, "Wideband patch antenna using multiple parasitic patches and its array application with mutual coupling reduction," *IEEE Access*, 2018.
14. Tang, M. C., et al., "Mutual coupling reduction using meta structures for wide band, dual-polarized, and high density patch arrays," *IEEE Trans. Antennas Propag.*, Vol. 65, No. 8, 3986–3998, Aug. 2017.
15. Henridass, A., K. Aswathy, et al., "Deployment of modified serpentine structure for mutual coupling reduction in MIMO antennas," *IEEE Antennas Wirel. Propag. Lett.*, Vol. 13, 277–280, 2014.
16. Mohsin, I., M. Karlsson, and O. Owais, "Design and implementation of a UWB six-port correlator for 6–9 GHz frequency band," *Microwave and Optical Technology Letters*, Vol. 55, No. 1, 190–193, Jan. 2013.
17. Wang, C. H. and Y. K. Chang, "Dual-band dual-polarized antenna array with flat-top and sharp cutoff radiation patterns for 2G/3G/LTE cellular bands," *IEEE Trans. Antennas Propag.*, Vol. 66, No. 11, 5907–5917, 2018.
18. Khanjari, S. P., S. Jarchi, and M. Mohammad-Taheri, "Compact and wideband planar loop antenna with microstrip to parallel strip balun feed using metamaterials," *AEU-International Journal of Electronics and Communications*, Vol. 111, 152883, 2019.
19. Andújar, A. and J. Anguera, "MIMO multiband antenna system combining resonant and nonresonant elements," *Microwave and Optical Technology Letters*, Vol. 56, No. 5, 1076–1084, 2014.
20. El Ouahabi, M., A. Zakriti, M. Essaaidi, A. Dkiouak, and E. Hanae, "A miniaturized dual-band MIMO antenna with low mutual coupling for wireless applications," *Progress In Electromagnetics Research C*, Vol. 93, 93–101, 2019.
21. Design Notes, "Return loss, reflection coefficient and VSWR," *High Frequency Electronics*, Apr. 2008.